SUPPLEMENTARY MATERIALS TO:

DATASET OF DAILY VERTICAL DISPLACEMENTS OBSERVED BY GPS BETWEEN 1994 AND 2023 FOR HYDROGEODETIC STUDIES OVER EUROPE

Anna Klos[1,2], Jürgen Kusche[2], Anne Springer[2], Artur Lenczuk[1], Yorck Ewerdwalbesloh[2], Christian Mielke[2], Susanna Werth[3,4], Jan Mikocki[1], Kinga Klos[1], Jakub Rados[1], Malgorzata Sieczak[1], Janusz Bogusz[1]

1) Military University of Technology, Warsaw, Poland

2) University of Bonn, Bonn, Germany

3) Virginia Tech, Blackburgs, USA

Contact e-mail: anna.klos@wat.edu.pl

Text S1. Modelling of GPS-observed vertical displacements.

We model the GPS-observed vertical displacements as a sum of deterministic and stochastic parts:

$$y(t) = x(t) + s(t) \tag{1}$$

with $x(t)$ and $s(t)$ being deterministic and stochastic components, respectively. To model the deterministic part, we use a constant velocity model presented by Bevis and Brown (2014), to which we add annual and semi-annual terms:

$$x(t) = x_0 + v(t - t_0) + \sum_{j=1}^{n_j} J_j H(t - t_j) + \sum_{k=1}^{2} \left[S_k \sin(\omega_k t) + C_k \cos(\omega_k t) \right] \tag{2}$$

where t_0 is the reference epoch, defined as the middle epoch of the time series, J_j is the magnitude of offset occurring in the t_j epoch, H is the Heaviside step function, k is the number of modeled frequencies, and $\omega_k = \frac{2\pi}{\tau_k}$ with τ_k=1 year and τ_k=1/2 year. To model the stochastic component $s(t)$, we use a combination of white noise and power-law noise, which has been widely recognized as the preferred noise combination for describing time series residuals between the original time series and the deterministic component (Williams et al., 2004; Santamaria-Gomez et al., 2011; Klos et al., 2018). Power-law noise is characterized by spectral index and amplitude.

Figure S1 presents the estimates of spectral indices and amplitudes of power-law noise for the set of 4,443 GPS-observed vertical displacements. By combining both these estimates, we group the GPS stations regionally into 11 regions, which are further used to stack and average the GPS-displacements in three pre-defined temporal resolutions for regional analyses and comparisons.

Text S2. A detailed description of the benchmarking results

Figure S2 shows the variance of the time series in the three temporal scales as introduced in the main body of the text. Most of the variance, over 70%, in the GPS time series originates from short-term displacements. Approximately 20-30% of the total signal, depending on the station, is generated at seasonal and long-term temporal scales, although at this stage we cannot clearly attribute this to either true signal or measurement noise. Motions at seasonal and long-term temporal scales are small and may be difficult to determine reliably, especially for stations where the variance of short-term temporal scale exceeds 90%. This is illustrated in Figure S3, which compares the time series of vertical displacements observed at the GPS station ZYWI (Zywiec, Poland), one of Europe's highest-quality permanent ("gold") stations, with those derived from the high-resolution hydrological model, CLM5 we use in the main body of the paper ("HYDOL"). The comparison is shown for the full time series as well as the extracted signal components at the three previously defined temporal scales: short-term, seasonal, and long-term. We note very good agreement between the vertical displacement signals from the GPS and the HYDOL model. This agreement is excellent for seasonal and long-term temporal scales, both in terms of the character of the observed changes, i.e., consistent increases and decreases of displacements at seasonal and long-term temporal scales, and their amplitude. Correlation coefficients between GPS and HYDOL are equal to 0.75 and 0.73 for the long-term and seasonal temporal scales, respectively. A large decrease in GPS-observed vertical displacements in 2010, which may be mistakenly identified as an offset, is also visible in the model. For short-term temporal scale, we note that the spread of the displacements observed by GPS is ten times greater than that predicted by HYDOL. Correlation coefficient between two time series is equal to 0.21.

Figure S4 presents correlation coefficients estimated between GPS-observed time series and time series derived from a model at the corresponding temporal scales. The high correlation coefficients between the GPS-observed and HYDOL-predicted displacements indicate an extreme similarity between these two time series on a long-term and seasonal temporal scales for all GPS locations across Europe. At long-term temporal scale, we find correlation between -1 (anticorrelation) and nearly 1, however, 40% of all time series achieve positive values higher than 0.5. For this temporal scale, we use a threshold of 0.3 for correlation coefficients to classify stations as benchmark dataset. In this way, 2,521 stations are classified as benchmark dataset. 33% of GPS stations included in the benchmark dataset are characterized by moderate positive correlation ranging from 0.3 to 0.5, and 67% by strong positive correlation ranging from 0.5 to 1.0. At the seasonal temporal scale, we find 90% of time series with positive correlation. Similarly to the long-term temporal scale, stations characterized by correlation coefficients higher than 0.3 are classified as benchmark dataset. In this way, a number of 3,401 stations is classified as the benchmark dataset for seasonal temporal scale. 19% of these stations show a moderate positive correlation ranging from 0.3 to 0.5, and 81% of these stations show strong positive correlation ranging from 0.5 to 1.0. For short-term temporal scale, fairly low correlation coefficients ranging from

-0.4 to 0.4 are found. 90% of stations achieve positive correlation coefficients. A number of 2,329 stations characterized by correlation coefficients higher than 0.1 are classified as the benchmark dataset for the short-term temporal scale.

We can conclude that GPS is sensitive to regional and local changes in hydrological loading. Long-term changes agree in the character, meaning that almost all increases and decreases present in the HYDOL-predicted displacements are also present in the GPS-observed displacements. Strong similarity is also observed for the seasonal temporal scale; both for annual amplitudes and phases. This is somewhat expected and consistent with previous studies that have demonstrated a potential of using GPS displacements to detect seasonal changes in the hydrosphere across Europe (starting with van Dam et al., 1997). Low, but positive correlation coefficients observed for the short-term temporal scale are also extremely encouraging. These values indicate that short-term signals, even hidden within the GPS noise, may arise from hydrosphere changes. At present, these changes are dominated by systematic errors and random errors in the GPS system or poorly modeled large-scale effects (Wdowinski et al. 1997; King et al. 2010). However, with the increasing accuracy of background models and the continuous evolution of GPS technique over time, this temporal scale may become increasingly reliable for estimating short-term changes in total water storage in the near future.

Figures S1-S4:

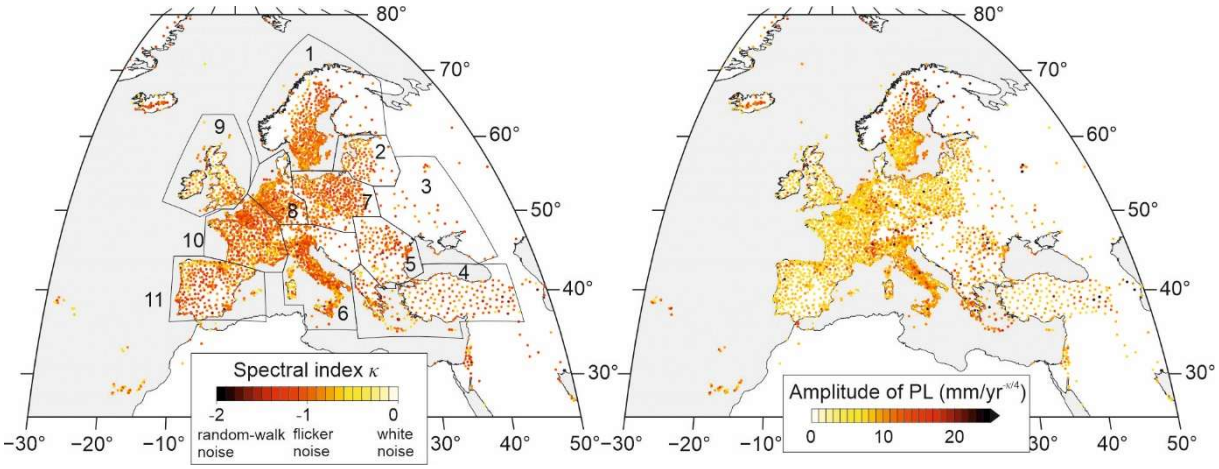

Fig. S1. Spectral indices and amplitudes of power-law noise estimated for a set of 4,443 GPS-observed vertical displacements over Europe.

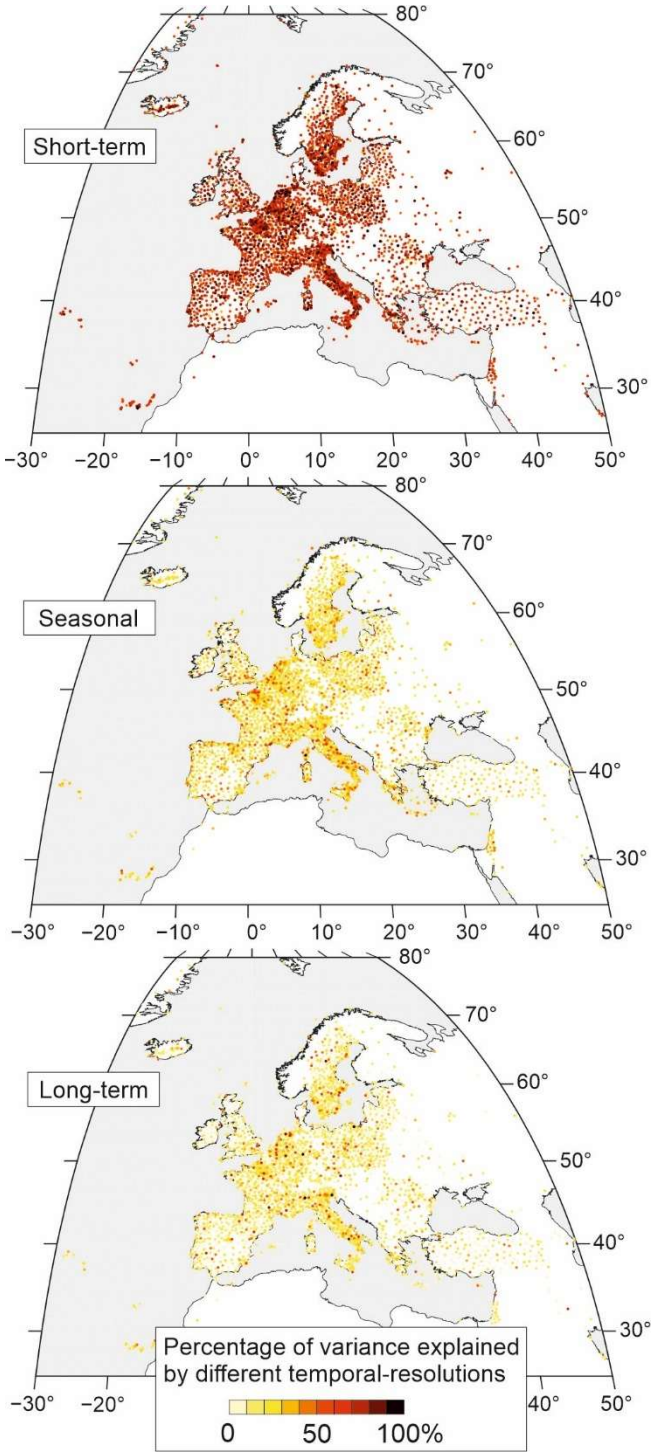

Fig. S2 Percentage of variance of GPS-observed displacements explained by different temporal scales. Note that the long-term temporal scale does not show a trend, but rather variability at scales longer than 1.1 years.

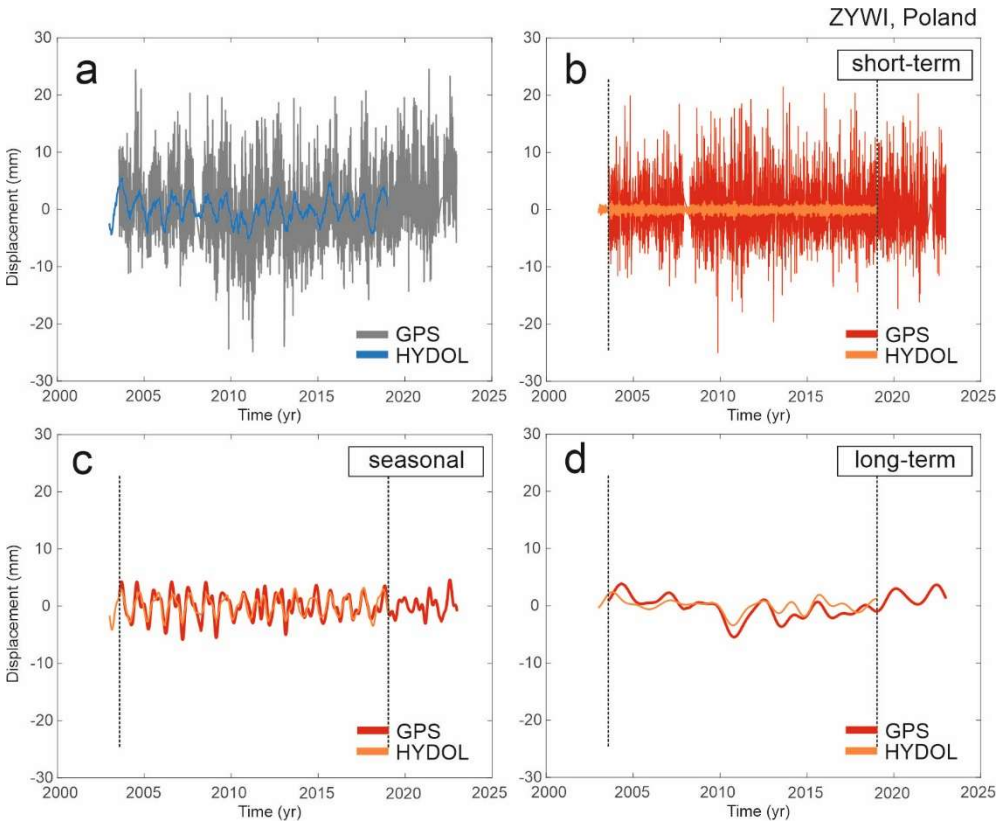

Fig. S3 (a) GPS-observed vertical displacements of the ZYWI GPS station (Zywiec, Poland), together with HYDOL-predicted displacements. (b-d) Short-term, seasonal, and long-term signal components determined using a wavelet-based decomposition of the displacement time series. Note that the linear trend has been removed from the time series.

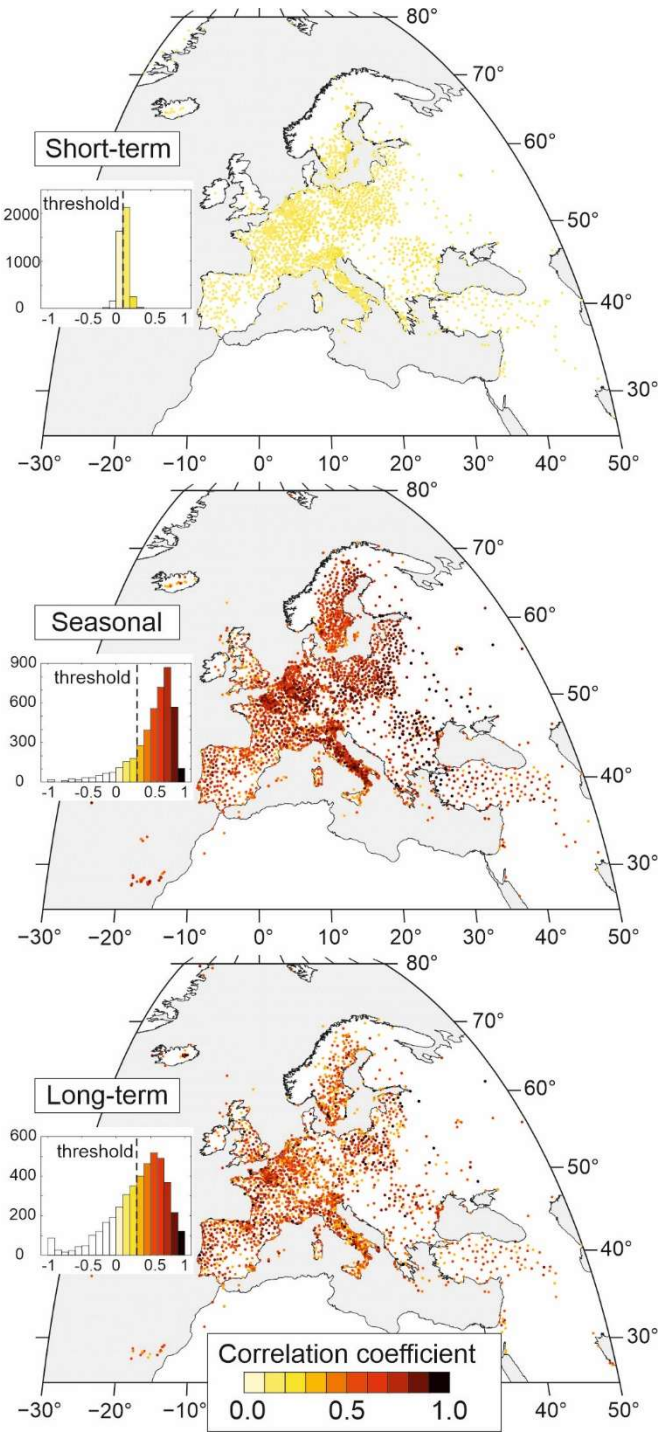

Fig. S4 GPS stations classified into benchmark dataset for Europe. Note that the histograms present all the correlation coefficients we obtain between the GPS-observed and HYDOL-predicted displacements. The maps show only those stations that we classify as benchmark dataset.

Table S1:

Table S1. SAR data and InSAR processing specifications.

Ascending Orbit Path ID	161 (eastern path)		59 (western path)	
ID of frames	156	151	155	160
# SAR images per frame	205	203	216	214
# Concatenated images along paths	408		430	
# Interferograms per path	598		553	
Total # images	848			
Total # interferograms	1152			
Maximum temporal baseline	350 days			
Perpendicular baseline	35 meters			
Multi-looking factor (range/azimuth direction)	31/6			
Average ground resolution	78 meters			
Scatterer coherence (PS/DS)	0.33 / 0.65			
# Concatenated images (time steps)	314			
Time Period of final VLM images	June 2, 2017 – March 2, 2024			
# Pixels in final VLM images	3820440			
Reference Frame	IGS-14			

References:

Antwi S.H., Rolston A., Linnane S., Getty D. (2022): Communicating water availability to improve awareness and implementation of water conservation: A study of the 2018 and 2020 drought events in the Republic of Ireland. Science of The Total Environment, 807, 2, 150865, DOI: 10.1016/j.scitotenv.2021.150865.

Bestakova Z., Kysely J., Lhotka O., Heilig M., Eitzinger J. (2024): Warm-season drying across Europe and its links to atmospheric circulation. Earth and Space Science, 11, 6, e2023EA003434, DOI: 10.1029/2023EA003434.

Chandanpurkar H.A., Famiglietti J.S., Gopalan K., Wiese D.N., Wada Y., Kakinuma K., Reager J.T., Zhang F. (2025): Unprecedented continental drying, shrinking freshwater availability, and increasing land contributions to sea level rise. Science Advances, 11, 30, DOI: 10.1126/sciadv.adx0298.

Gerdener H., Kusche J., Schulze K., Doll P., Klos A. (2023a): The global land water storage data set release 2 (GLWS2.0) derived via assimilating GRACE and GRACE-FO data into global hydrological model. Journal of Geodesy, 97, 73, DOI: 10.1007/s00190-023-01763-9.

Junquera V., Hormaza J.I., Rubenstein D.I., Jimenez Gavilan P. (2025): Severe water crisis in southern Spain under expanding irrigated agriculture: A multidimensional drought analysis. PNAS, 122, 39, DOI: 10.1073/pnas.2508055122.

Montanari A., Nguyen H., Rubinetti S., Ceola S., Galelli S., Rubino A., Zanchettin D. (2023): Why the 2022 Po River drought is the worst in the past two centuries. Science Advances, 9, 32, DOI: 10.1126/sciadv.adg8304.

NOAA National Centers for Environmental Information (NCEI), 2025, Global Drought Narrative, from https://www.ncei.noaa.gov.

OECD (2025), Adapting the Paris Metropolitan Area to a Water-Scarce Future, OECD Publishing, Paris, https://doi.org/10.1787/00a103f8-en.

Passos M.V., Kan J.-C., Destouni G., Barquet K., Kalantari Z. (2024): Identifying regional hotspots of heatwaves, droughts, floods, and their co-occurrences. Stochastic Environmental Research and Rosk Assessment, 38, 3875-3893, DOI: 10.1007/s00477-024-02783-3.

Rezaei A., Karami K., Tilmes S., Moore J.C. (2024): Future water storage changes over the Mediterranean, Middle East, and North Africa in response to global warming and stratospheric aerosol intervention. Earth System Dynamics, 15, 1, DOI: 10.5194/esd-15-91-2024.